IJMMM International Journal of Minerals, Metallurgy and Materials 矿物冶金与材料学报（英文版）

Effects of shape and particle size on the photocatalytic kinetics and mechanism of nano-CeO_2

Zixiang Cui, Lu Zhang, Yongqiang Xue, Ya'nan Feng, Mengying Wang, Jiaojiao Chen, Boteng Ji, Chenyu Wang, and Yidi Xue

Cite this article as:
Zixiang Cui, Lu Zhang, Yongqiang Xue, Ya'nan Feng, Mengying Wang, Jiaojiao Chen, Boteng Ji, Chenyu Wang, and Yidi Xue, Effects of shape and particle size on the photocatalytic kinetics and mechanism of nano-CeO_2, *Int. J. Miner. Metall. Mater.*, 29(2022), No. 12, pp. 2221-2231. https://doi.org/10.1007/s12613-021-2332-0

View the article online at SpringerLink or IJMMM Webpage.

Articles you may be interested in

Jing Zhou, Dan-dan Nie, Xian-bo Jin, and Wei Xiao, Controllable nitridation of Ta_2O_5 in molten salts for enhanced photocatalysis, *Int. J. Miner. Metall. Mater.*, 27(2020), No. 12, pp. 1703-1710. https://doi.org/10.1007/s12613-020-2050-z

Guo-qing Li, Pu-kang Wen, Chen-qiang Gao, Tian-yi Zhang, Jun-yang Hu, Yu-hao Zhang, Shi-you Guan, Qing-feng Li, and Bing Li, Effects of CeO_2 pre-calcined at different temperatures on the performance of Pt/CeO_2–C electrocatalyst for methanol oxidation reaction, *Int. J. Miner. Metall. Mater.*, 28(2021), No. 7, pp. 1224-1232. https://doi.org/10.1007/s12613-020-2076-2

Hai-xia Liu, Meng-yuan Teng, Xu-guang Wei, Tian-duo Li, Zai-yong Jiang, Qing-fen Niu, and Xu-ping Wang, Mosaic structure ZnO formed by secondary crystallization with enhanced photocatalytic performance, *Int. J. Miner. Metall. Mater.*, 28(2021), No. 3, pp. 495-502. https://doi.org/10.1007/s12613-020-2033-0

Xiong-feng Zeng, Jian-sheng Wang, Ying-na Zhao, Wen-li Zhang, and Meng-huan Wang, Construction of TiO_2-pillared multilayer graphene nanocomposites as efficient photocatalysts for ciprofloxacin degradation, *Int. J. Miner. Metall. Mater.*, 28(2021), No. 3, pp. 503-510. https://doi.org/10.1007/s12613-020-2193-y

Alexander M. Klyushnikov, Rosa I. Gulyaeva, Evgeniy N. Selivanov, and Sergey M. Pikalov, Kinetics and mechanism of oxidation for nickel-containing pyrrhotite tailings, *Int. J. Miner. Metall. Mater.*, 28(2021), No. 9, pp. 1469-1477. https://doi.org/10.1007/s12613-020-2109-x

Rui-qi Yang, Na Liang, Xuan-yu Chen, Long-wei Wang, Guo-xin Song, Yan-chen Ji, Na Ren, Ya-wei Lü, Jian Zhang, and Xin Yu, Sn/Sn_3O_{4-x} heterostructure rich in oxygen vacancies with enhanced visible light photocatalytic oxidation performance, *Int. J. Miner. Metall. Mater.*, 28(2021), No. 1, pp. 150-159. https://doi.org/10.1007/s12613-020-2131-z

IJMMM WeChat

QQ author group

International Journal of Minerals, Metallurgy and Materials
Volume 29, Number 12, December 2022, Page 2221
https://doi.org/10.1007/s12613-021-2332-0

Effects of shape and particle size on the photocatalytic kinetics and mechanism of nano-CeO_2

Zixiang Cui ✉, *Lu Zhang*, *Yongqiang Xue*, *Ya'nan Feng*, *Mengying Wang*, *Jiaojiao Chen*, *Boteng Ji*, *Chenyu Wang*, *and Yidi Xue*

Department of Chemistry, College of Chemistry and Chemical Engineering, Taiyuan University of Technology, Taiyuan 030024, China
(Received: 27 May 2021; revised: 18 July 2021; accepted: 19 July 2021)

Abstract: Nanomaterials have been widely applied to many fields because of their excellent photocatalytic performance. The performance is closely related to the catalytic kinetics, but it is not completely clear about the influencing regularities of shape and particle size on the photocatalytic kinetics of nanomaterials and the photocatalytic kinetic mechanism. In this paper, nano-CeO_2 with different shapes and particle sizes were prepared, the kinetic parameters of adsorption and photocatalytic degradation were determined, and the effects of shape and particle size on the kinetics of adsorption and photocatalysis and photocatalytic mechanism were discussed. The results show that the shape and particle size have significant influences. With the decreases of diameter, the performances of adsorption and photocatalysis of nano-CeO_2 are improved; and these performances of spherical nano-CeO_2 are greater than those of linear nano-CeO_2. The shape and particle size have no effects on the kinetic order and mechanism of the whole photocatalytic process. Then a generalized mechanism of photocatalytic kinetics of nanomaterials was proposed and the mechanism rate equation was derived. Finally, the conclusion can be drawn: the desorption of photodegradation products is the control step of photocatalytic kinetics, and the kinetic order of photocatalytic degradation reaction is 1. The mechanism is universal and all nanomaterials have the same photocatalytic kinetic mechanism and order.

Keywords: nanoparticles; photocatalysis; particle size; shape; kinetics

1. Introduction

Because nanomaterials have large oxygen vacancies and specific surface area [1], they have excellent photocatalytic performance compared with the corresponding bulk materials [2–4]. Therefore, they have shown broad application prospects in wastewater treatment [5–7], solar cells [8–10], and ultraviolet shielding agents [11–13]. Semiconductor materials such as ZnS, Fe_2O_3, TiO_2, and CeO_2 have been used to remove organic pollutants from various pollution sources due to their excellent photoactivity [14–17]. Among them, CeO_2 is a relatively stable rare earth metal oxide and has good oxygen storage and release capabilities. As its valence changes, oxygen vacancies or lattice defects are formed by losing oxygen or electrons. The crystal is a cubic fluorite structure. Nano-CeO_2 has shown potential application prospects in the field of wastewater treatment and photodegradation due to its unique biocompatibility, chemical inertness, and strong oxidizing ability. At the same time, it has received widespread attention. When nano-CeO_2 is used to treat organic wastewater, it can adsorb organic substances. After light irradiation, it can decompose organic substances that are difficult to decompose into inorganic substances such as water and carbon dioxide without secondary pollution [18], thus achieving the purpose of environmental protection.

It is widely known that the photocatalytic performance of nanomaterials is determined by photocatalytic kinetics, while the photocatalytic kinetics of nanomaterials has a unique kinetic mechanism and influence regularities. Among them, the shape and particle size of nanomaterials have a significant influence on their photocatalytic kinetics. Therefore, the study of the generalized photocatalytic kinetics mechanism of nanomaterials and the generalized influencing regularities of shape and particle size on photocatalytic kinetics can provide important theoretical guidance and reference value for the research and applications of nanomaterials in the field of photocatalysis!

The effects of shape and particle size on the photocatalytic kinetics of nanomaterials have always been one of the hotspots in the field of nanomaterials. At present, a lot of literature has reported the above influence. For example, Ling *et al.* [19] synthesized composites of humic acid-supported CeO_2 nano-sheet with the size of 100–500 nm by solvothermal method. The obtained composites have excellent adsorption performance for congo red, and the adsorption behavior follows a pseudo-second-order kinetic model. Tian *et al.* [20] prepared nano-$NiCo_2O_4$ with different shapes and measured the removal efficiency of methyl orange solution. The ad-

✉ Corresponding author: Zixiang Cui E-mail: czxlw2018@163.com

sorption capacity followed the following order: $NiCo_2O_4$ nanorods > balsam-like $NiCo_2O_4$ > rose-like $NiCo_2O_4$ > $NiCo_2O_4$ nanoribbons > $NiCo_2O_4$ flowerlike nanostructures > dandelion-like $NiCo_2O_4$ spheres and their adsorption behaviors all conform to the pseudo-second-order kinetic model. Gao *et al*. [21] used the hydrolysis-deposition technique to immobilize the nano-TiO_2 on the surface of DBPCs (Diatomite-based porous ceramics), the main crystalline phase of TiO_2 calcined at 650°C was anatase, and the average grain size was 8.3 nm. The removal rate of formaldehyde was increased by 32.1% under the same conditions compared with an air purifier with nano-TiO_2/ nickel-foam photocatalyst cores. Moreover, the photocatalytic degradation process of formaldehyde can be characterized by pseudo-first-order model. Ji *et al*. [22] prepared TiO_2 nano-films with different shapes on the surface of titanium mesh by hydrothermal method, the flower-like TiO_2/Ti-2, the mixture of nano-sheet and nanowire like TiO_2/Ti-4, the nanowire like TiO_2/Ti-6, and the nanowire like TiO_2/Ti-8 with higher density were synthesized at different NaOH concentrations (2, 4, 6, 8 M). The rate of degradation of ethylene within 60 min was 54.44%, 85.92%, 95.62%, and 96.94%, respectively. The ethylene photodegradation reaction all conforms to the pseudo-first-order kinetics model. Ghasemi *et al*. [23] studied the heterogeneous photocatalytic degradation of organic pollutants in refinery wastewater under ultraviolet light irradiation by nano-TiO_2 supported on Fe-ZSM-5 molecular sieve. For the TiO_2/Fe-ZSM-5 concentration of 1, 2, 3, and 4 $g \cdot L^{-1}$, the fitted reaction data follow the pseudo-first-order kinetic model. Nasseh *et al*. [24] synthesized $FeNi_3/SiO_2$/ZnO magnetic nano-composite for the first time. Under the conditions of pH = 9, photocatalyst loading of 0.02 $g \cdot L^{-1}$, contact time of 200 min, and initial tetracycline concentration of 15 $mg \cdot L^{-1}$, tetracycline was completely degraded. The degradation kinetics of tetracycline follows the pseudo-first-order kinetic model. In brief, the adsorption behavior agrees with the pseudo-second-order kinetic model, while the photocatalytic degradation process is consistent with the pseudo-first-order Langmuir-Hinshelwood kinetics model. However, there is no satisfactory explanation for this universal regularity at present. In other words, the photocatalytic kinetic mechanism of nanomaterials is still unclear, which will seriously influence the research and applications of nanomaterials in the photocatalytic field.

We found that most of the nano-CeO_2 is prepared by the hydrothermal method, and the purity, homogeneity, and dispersion of the nanoparticles prepared by the hydrothermal method are relatively high. Therefore, in this paper, nano-CeO_2 with different shapes and particle sizes were prepared by hydrothermal method, then the kinetic parameters of photocatalytic degradation of Rhodamine B by nano-CeO_2 were determined, and the influencing regularities of shape and particle size on the photocatalytic kinetics and photocatalytic mechanism of nano-CeO_2 were discussed. On this basis, the generalized photocatalytic kinetics mechanism of nanomaterials was proposed, and the mechanism rate equation was derived. The experimental results are compared and analyzed to discuss the correctness and universality of the mechanism of the photocatalytic kinetics mechanism.

2. Experimental

2.1. Preparation of spherical nano-CeO_2

A certain amount of $Ce(NO_3)_3 \cdot 6H_2O$ (AR, was purchased from Tianjin Guangfu Fine Chemical research institute) was dissolved in distilled water. The resulting solution was added 120 mL ethylene glycol (AR, was purchased from Tianjin Yongda Cemical Reagent CO., LTD.) and stirred to make the mixture a homogeneous solution. Then the solution was transferred to a 200 mL hydrothermal synthesis kettle and put into an oven for reaction. After natural cooling, the reaction kettle was taken out, centrifuged, and washed three times with water and ethanol (AR, was purchased from Tianjin Guangfu Technology Development Co., Ltd.). Finally, the washed white solid was put into an oven at 60°C, dried for 120 min, and taken out for grinding. Spherical nano-CeO_2 samples with different particle sizes were obtained by controlling the concentration of cerium source, reaction temperature, and reaction time.

2.2. Preparation of linear nano-CeO_2

0.5 M $CeCl_3 \cdot 7H_2O$ solution (AR, was purchased from Tianjin Guangfu Fine Chemical research institute) was prepared. A certain volume of the above solution was mixed with 12.5 mL ammonia water (AR, Tianjin Beichen Fangzheng Reagent Factory) and then stirred for 30 min to form a purple mixture. The resulted mixture was washed twice with water and then centrifuged. The precipitate was dissolved in 50 mL deionized water, then transferred to a 200 mL hydrothermal synthesis kettle and put into an oven for reaction. After natural cooling, the reaction kettle was taken out, centrifuged, and washed three times with water and ethanol (AR, was purchased from Tianjin Guangfu Technology Development Co., Ltd.). Finally, the washed white solid was put into an oven at 60°C, dried for 120 min, and taken out for grinding. Linear nano-CeO_2 samples with different cross-sectional diameters were obtained by controlling the volume of $CeCl_3 \cdot 7H_2O$.

2.3. Characterization of nano-CeO_2

A scanning electron microscope (SEM) (JEOL, Germany, JSM-6701F) was used to analyze the surface shapes of the samples and the shapes and particle sizes of the prepared nano-CeO_2 were observed from the SEM images. The type and crystal form of the samples were measured using a Shimadzu 6000 X-ray diffractometer (Cu K_α, $\lambda = 0.154178$ nm). Test conditions: step size, scanning range, and scanning speed were 0.02°, 20° to 80°, and $8.0° \cdot min^{-1}$.

2.4. Adsorption and photocatalytic experiments

CeO_2 nanoparticles of the same quality were added to different dyes of the same concentration and performed lightproof adsorption at 25°C until the concentration of the solution no longer changes. It shows that the dark adsorption equilibrium was reached, which also was the starting point of

photocatalysis. Then a 30 W UV LED lamp (Dongguan Senxia Electronic Technology Co., Ltd., China, 365M) was turned on as the light source. The distance between the lamp and the solution was set to 10 cm and the photodegradation was started. A certain amount of organic dye was taken for a centrifugal separation every 30 min and the corresponding absorbance was measured. Until the concentration of dyes almost no longer changes, that is, the end of photocatalysis was reached.

2.5. Data processing

2.5.1. Determination of adsorption rate

The adsorption rates (α) of RhB on spherical and linear nano-CeO_2 with different diameters at different stages of dark adsorption are calculated by Eq. (1):

$$\alpha = (c_0 - c_t)/c_0 \times 100\% \quad (1)$$

where c_0 and c_t are the concentration of the dye solution at the initial and the time t, the unit is mg·L^{-1}.

2.5.2. Determination of degradation rate

The absorbance was measured at the maximum absorption wavelength of the degraded dye and then the degradation rate was calculated. The formula for degradation rate (η) is shown in Eq. (2):

$$\eta = (c_0' - c_t')/c_0' \times 100\% \quad (2)$$

where c_0' and c_t' are the concentration of the dye solution at the initial and the time t of photocatalysis, the unit is mg·L^{-1}.

2.5.3. Determination of adsorption kinetics order

To further study the adsorption process, the pseudo-first-order adsorption equation proposed by Lagergren [25] in 1898 (Eq. (3)) and Ho and McKay's [26] pseudo-second-order adsorption equation in 1999 (Eq. (4)) were used.

$$dq_t/dt = k_1(q_e - q_t) \quad (3)$$

$$dq_t/dt = k_2(q_e - q_t)^2 \quad (4)$$

Among them, t, q_t, q_e, k_1, k_2 are time, instantaneous adsorption capacity, equilibrium adsorption capacity, the pseudo-first-order adsorption rate constant, and the pseudo-second-order adsorption rate constant, and the units are min, 1, 1, min^{-1}, and mg·mg^{-1}·min^{-1}, respectively.

Integral deformation of Eq. (3) and Eq. (4) are:

$$q_t = q_e(1 - e^{-k_1 t}) \quad (5)$$

$$\frac{t}{q_t} = \frac{t}{q_e} + \frac{1}{k_2 q_e^2} \quad (6)$$

The linearized form of Eq. (5) can be described using Eq. (7):

$$\ln\left(1 - \frac{q_t}{q_e}\right) = -k_1 t \quad (7)$$

The adsorption kinetic order was determined by comparing the square of linear correlation coefficients (R^2) obtained by fitting $\frac{t}{q_t}$ vs. t in Eq. (6) and $\ln\left(1 - \frac{q_t}{q_e}\right)$ vs. t in Eq. (7). According to their slope or intercept, the adsorption rate constant can be obtained.

2.5.4. Determination of the order of photocatalytic kinetics

To further study the photodegradation of RhB, according to the Langmuir–Hinshelwood first-order kinetic model [27–29] and the second-order kinetic equation, the experimental data were fitted by the Eq. (8) and Eq. (9) to calculate the photodegradation rate constant:

$$\ln\left(\frac{c_0'}{c_t'}\right) = k_{app} t \quad (8)$$

$$\frac{1}{c_t'} = k_2' t + \frac{1}{c_0'} k_2 \quad (9)$$

where c_0', c_t', k_{app}, k_2' are the concentration of the dye when the dark adsorption reaches equilibrium(the concentration at the beginning of photocatalysis), the concentration of the dye at the time t, the photocatalytic apparent rate constant, and the second-order rate constant, the units are mg·L^{-1}, mg·L^{-1}, min^{-1}, and L·mg^{-1}·min^{-1}, respectively.

The photocatalytic kinetic order was determined by comparing the square of R^2 obtained by fitting $\ln\left(\frac{c_0'}{c_t'}\right)$ vs. t in Eq. (8) and $\frac{1}{c_t'}$ vs. t in Eq. (9). According to its slope, the photocatalytic rate constant can be obtained.

3. Results and discussion

3.1. Preparation results of nano-CeO_2 with different shapes and particle sizes

In the preparation of spherical nano-CeO_2, the particle size decreases with the increase of cerium source concentration and increases with the increase of reaction temperature and time. In the preparation of linear nano-CeO_2, as the volume of the cerium source increases, the cross-sectional diameter decreases first and then increases. Under the same conditions of hydrothermal temperature, as the hydrothermal time increases, the cross-sectional diameter shows an increasing trend. The specific preparation conditions of each particle size are shown in Tables 1 and 2.

Table 1. Specific preparation conditions of each particle size of spherical nano-CeO_2

Size / nm	$m(Ce(NO_3)_3 \cdot 6H_2O)$ / g	$V(H_2O)$ / mL	T / °C	t / min
58.2	4.00	4	150	200
80.2	4.00	4	160	200
97.3	2.17	10	160	300
125.1	2.17	10	140	1080
150.2	2.17	10	140	600

Table 2. Specific preparation conditions of each cross-sectional diameter of linear nano-CeO_2

Size / nm	$C(CeCl_3 \cdot 7H_2O)$ / M	$V(CeCl_3 \cdot 7H_2O)$ / mL	$V(NH_3)$ / mL	T / °C	t / h
25.9	0.5	40.0	12.5	180	8
38.0	0.5	25.0	12.5	180	12
49.1	0.5	25.0	12.5	180	24
59.2	0.5	60.0	12.5	180	8
77.6	0.5	75.0	12.5	180	8

The shapes and particle sizes of the nano-CeO_2 samples were characterized by SEM, as shown in Figs. 1 and 2. The samples in Fig. 1 are all regular and relatively dispersed spherical, and their particle sizes are 58.2 nm, 80.2 nm, 97.3 nm, 125.1 nm, and 150.2 nm, respectively. The samples in Fig. 2 are all nanowire-shaped CeO_2 with good dispersion, and their cross-sectional diameters are 25.9 nm, 38.0 nm, 49.1 nm, 59.2 nm, and 77.6 nm, respectively. The XRD patterns of spherical and linear nano-CeO_2 with different diameters (Fig. 3) indicate the existence of spherical and linear nano-CeO_2. The diffraction peaks of spherical and linear nano-CeO_2 corresponded to the (111), (200), (220), (311) planes.

3.2. Experimental results of photocatalytic selectivity

To use the dye with the best photocatalytic effect, the photocatalytic selectivity of nano-CeO_2 was investigated. Then the photocatalytic degradation of Rhodamine B (RhB), Methyl orange (MO), and Methylene blue (MB) was studied by using linear nano-CeO_2 with a diameter of 38.0 nm as a photocatalyst. The degradation rates of nano-CeO_2 to different dyes were calculated by Eq. (2), as shown in Fig. 4. It displays that nano-CeO_2 has different degradation rates for different dyes. Therefore, it is feasible to use nano-CeO_2 for photocatalytic degradation of RhB.

3.3. Effects of shape and particle size on the adsorption kinetics of nano-CeO_2

According to the conclusion drawn in Fig. 4, RhB was selected as the dye to study the effects of shape and particle size on adsorption and photocatalytic kinetics of nano-CeO_2. The adsorption rates of spherical and linear nano-CeO_2 with different diameters were calculated by Eq. (1), as shown in Fig. 5.

It can be seen that the change regularity is the same. The adsorption rates increase sharply in the beginning, then in-

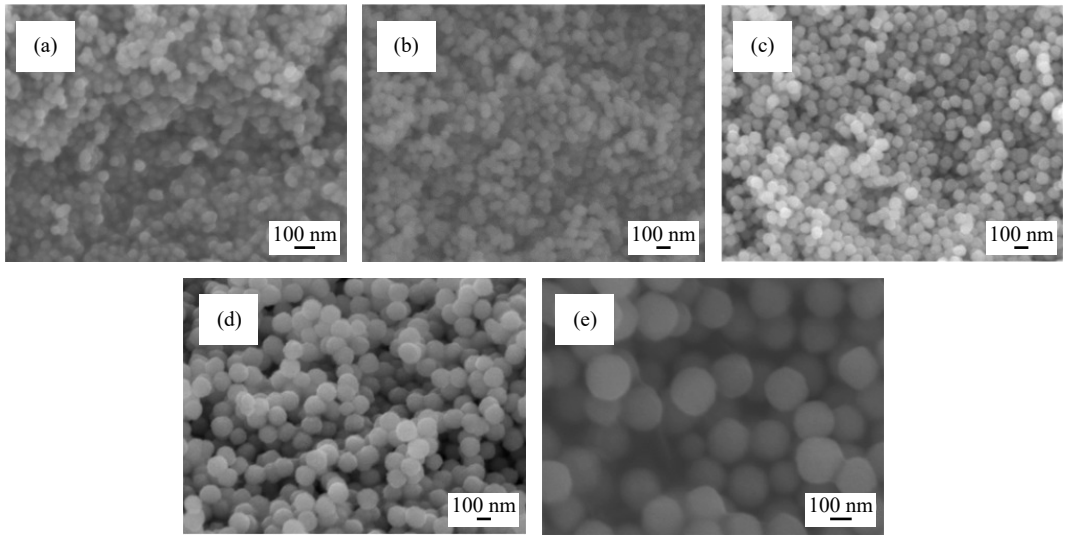

Fig. 1. SEM images of spherical nano-CeO_2 with different particle sizes: (a) 58.2 nm; (b) 80.2 nm; (c) 97.3 nm; (d) 125.1 nm; (e) 150.2 nm.

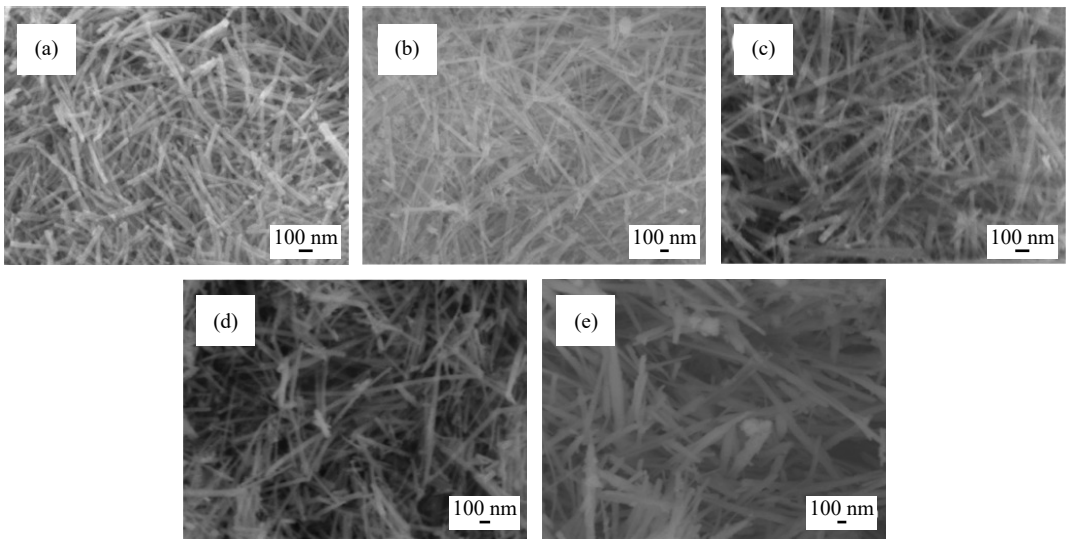

Fig. 2. SEM images of linear nano-CeO_2 with different cross-sectional diameters: (a) 25.9 nm; (b) 38.0 nm; (c) 49.1 nm; (d) 59.2 nm; (e) 77.6 nm.

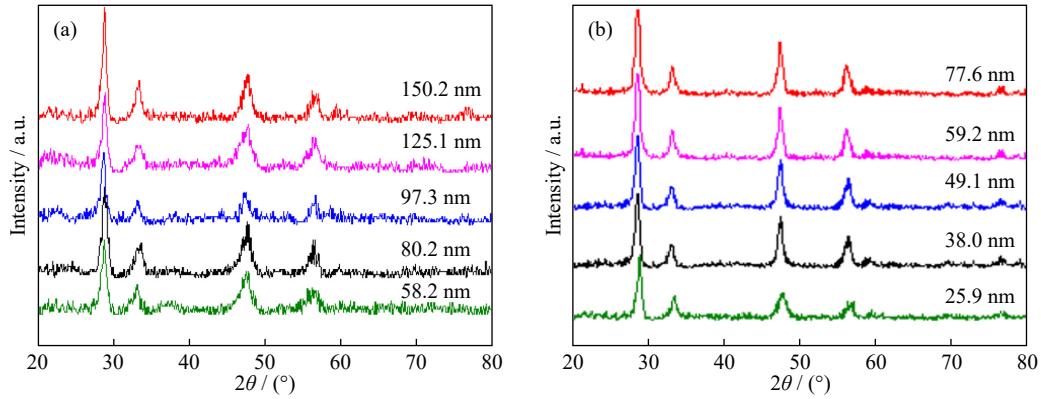

Fig. 3. XRD patterns of nano-CeO_2 with different diameters: (a) spherical nano-CeO_2; (b) linear nano-CeO_2.

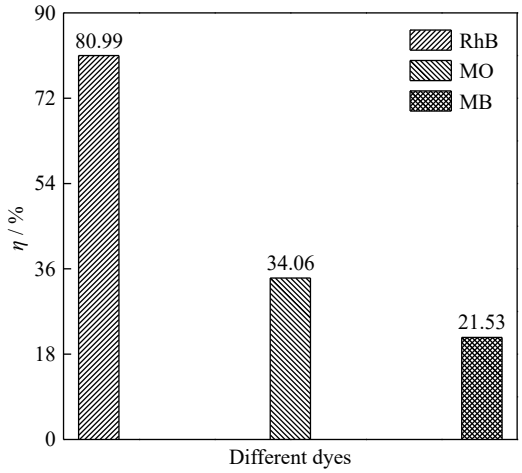

Fig. 4. Degradation rates of different dyes.

crease slowly with the extension of time, and finally reach the adsorption equilibrium. The adsorption rates become constants at this moment. This is because there are many adsorption sites on the nanoparticles and higher dye concentration in solution at first, which can adsorb more dye molecules, and the initial adsorption rate increases sharply. As time goes by, the adsorption sites are gradually occupied by dye molecules, and the concentration of the dye in the solution also gradually decreases. Therefore, the adsorption rate slowly increases and finally reaches equilibrium. In addition, Fig. 5 also shows that the adsorption rate increases with the decrease of particle size.

To further study the adsorption process, the experimental results were fitted by Eqs. (6) and (7). The corresponding fitting curves of the pseudo-first-order and pseudo-second-order kinetics are shown in Figs. 6 and 7. The relevant parameters of the fitted kinetic equation are shown in Table 3. The results show that the R^2 of pseudo-second-order adsorption kinetics is significantly higher than pseudo-first-order adsorption kinetics, indicating that the adsorption processes of RhB by spherical and linear nano-CeO_2 with different diameters follow the pseudo-second-order adsorption kinetics.

The relationships between the equilibrium adsorption rate (α_e) and the reciprocal of the diameter ($1/d$), and the logarithm of pseudo-second-order adsorption rate constant ($\ln k_2$) and $1/d$ are shown in Fig. 8. It shows that that $\ln k_2$ has a good linear relationship with the $1/d$, and α_e and $\ln k_2$ increase with the decreases of particle size. This is because the surface energy of small size nanoparticles is relatively large and cannot be ignored, which makes the adsorption rate constant of nanoparticles increase accordingly [30]. In addition, the α_e and $\ln k_2$ of spherical nano-CeO_2 are significantly higher than those of linear nano-CeO_2 when the diameters are the same. This is because spherical nanoparticles expose more adsorption sites than linear nanoparticles, and RhB is more easily adsorbed on the surface of spherical nanoparticles.

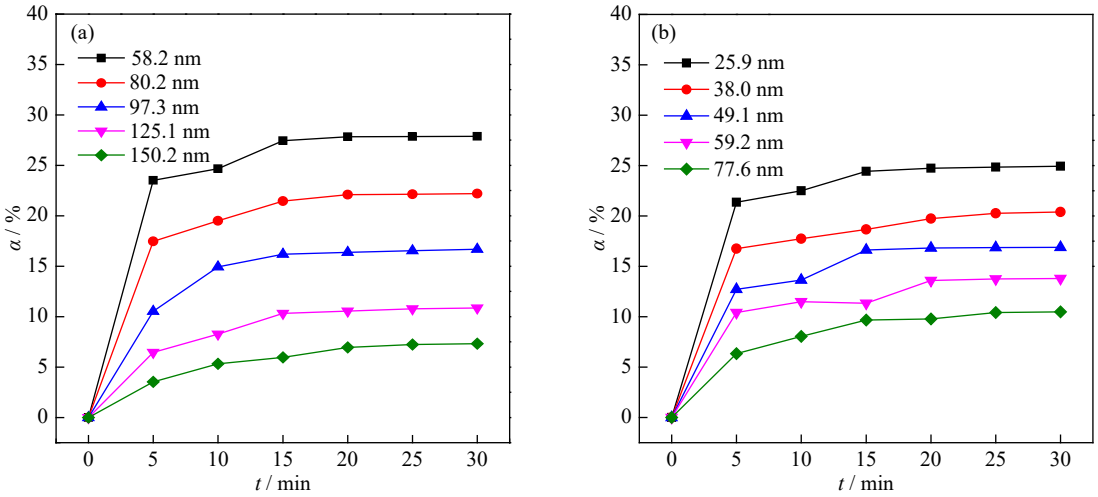

Fig. 5. Adsorption rate of RhB by nano-CeO_2: (a) spherical nano-CeO_2; (b) linear nano-CeO_2.

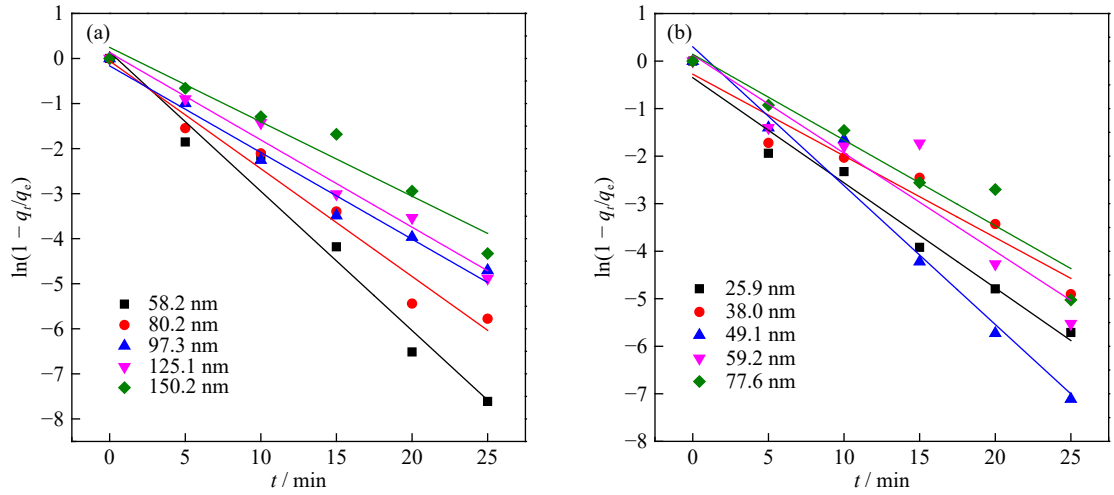

Fig. 6. Fit plots of the pseudo-first-order kinetic equation for the adsorption of RhB by nano-CeO_2 with different diameters: (a) spherical nano-CeO_2; (b) linear nano-CeO_2.

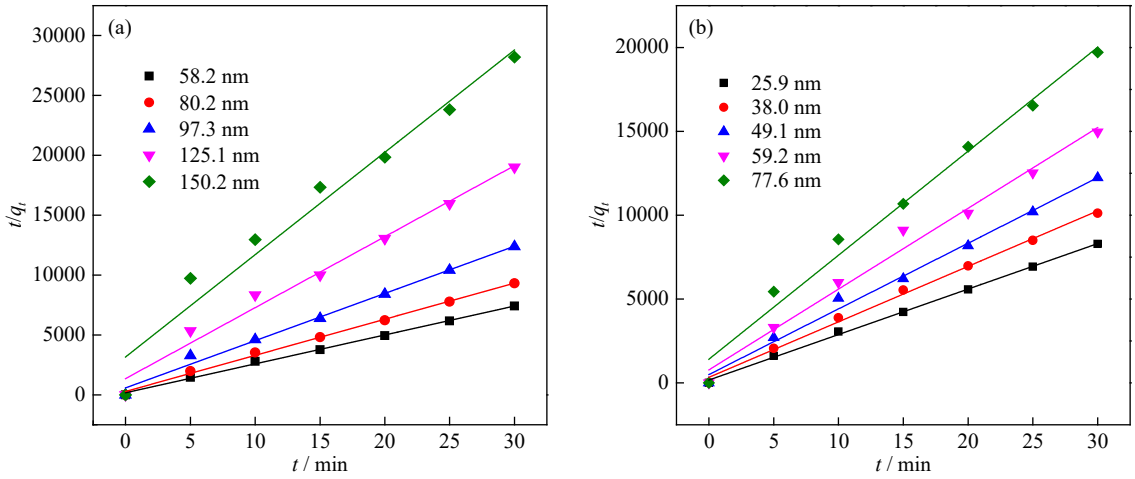

Fig. 7. Fit plots of the pseudo-second-order kinetic equation for the adsorption of RhB by nano-CeO_2 with different diameters: (a) spherical nano-CeO_2; (b) linear nano-CeO_2.

Table 3. Adsorption kinetic parameters for RhB adsorption on nano-CeO_2

Shape	Size / nm	Pseudo-first-order kinetics			Pseudo-second-order kinetic		
		q_e	k_1 / min^{-1}	R^2	q_e	k_2 / ($mg \cdot mg^{-1} \cdot min^{-1}$)	R^2
Spherical nano-CeO_2	58.2	0.004050	0.30896	0.96581	0.004142	341.37	0.99753
	80.2	0.003224	0.23911	0.96621	0.003315	325.78	0.99670
	97.3	0.002424	0.19230	0.97419	0.002536	268.30	0.99037
	125.1	0.001578	0.19361	0.97839	0.001687	260.21	0.98018
	150.2	0.001100	0.16512	0.94060	0.001170	231.10	0.95558
Linear nano-CeO_2	25.9	0.003622	0.22114	0.97115	0.003686	434.46	0.99837
	38.0	0.002964	0.17180	0.92980	0.003021	342.49	0.99593
	49.1	0.002452	0.29202	0.96230	0.002553	310.26	0.99145
	59.2	0.002004	0.20658	0.87146	0.002075	300.97	0.98384
	77.6	0.001522	0.18029	0.90994	0.001612	273.00	0.98221

It can be concluded from above that the shape and particle size of nano-CeO_2 only affect the kinetic parameters of adsorption, but not the order of adsorption kinetics.

3.4. Effects of shape and particle size on the photocatalytic kinetics of nano-CeO_2

When the dark adsorption reached equilibrium, a 30 W UV LED lamp was used as the light source for photocatalytic degradation of RhB. The instantaneous degradation rates of the photocatalytic degradation of RhB with spherical and linear nano-CeO_2 of different diameters are shown in Fig. 9. The photocatalytic degradation rates increase sharply in the beginning, then slowly increase, and reach the degradation equilibrium as time goes by. Eventually, the degradation

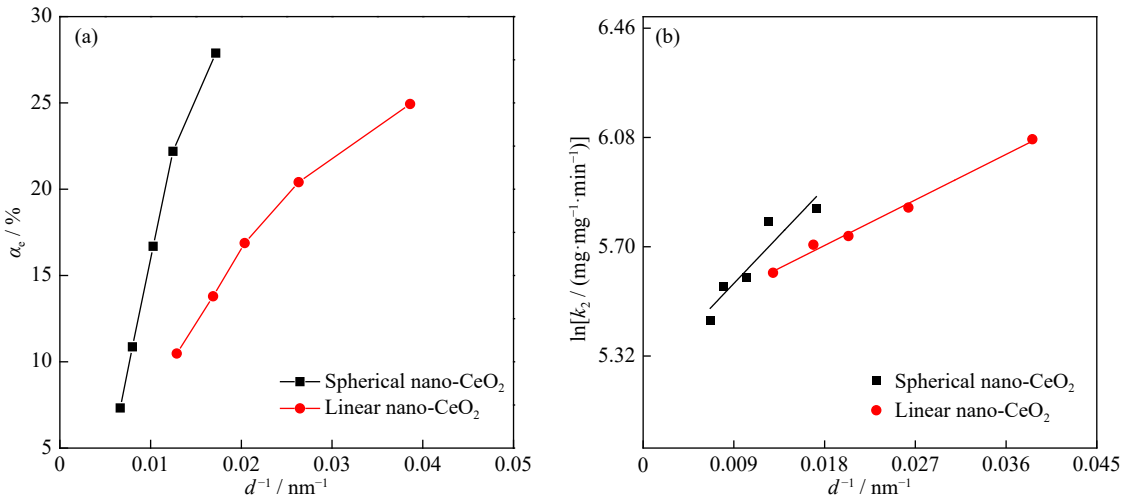

Fig. 8. Relationships between α_e and 1/d (a), and (b) lnk_2 and 1/d.

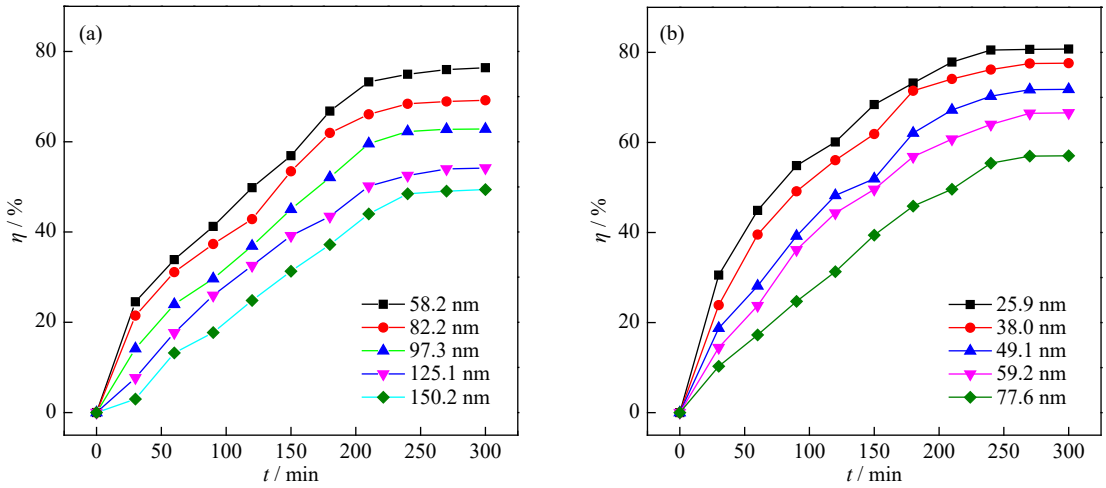

Fig. 9. Instantaneous degradation rate of nano-CeO_2 photocatalytic degradation of RhB: (a) spherical nano-CeO_2; (b) linear nano-CeO_2.

rates become constants. Light energy was absorbed by nanoparticles under light conditions. Next electron transitions were produced, and electron-hole pairs were generated. Therefore, the rapid degradation of dye molecules can be achieved. However, the electron-hole pairs recombined with the extension of time, and the continuous degradation of dye molecules also leads to the gradual decrease of the dye molecules adsorbed on the surface of the nanoparticles. Therefore, the photocatalytic degradation efficiency gradually slows down and finally reaches the degradation equilibrium. In addition, when the shape is the same, the smaller the particle size is, the higher the photocatalytic degradation rate is, and spherical nanoparticles with smaller particle sizes can provide more catalytic active centers [31], which is beneficial to the photocatalytic reaction on its surface.

To further study the photodegradation of RhB, the experimental data were fitted by Eqs. (8) and (9), as shown in Figs. 10 and 11. The corresponding parameters are shown in Table 4. It can be seen that compared with the second-order kinetics, the fit plots of the Langmuir-Hinshelwood first-order kinetics have better linear relationships and higher values of R^2, indicating that the photocatalytic kinetics of RhB by nano-CeO_2 conforms to the first-order kinetic model. In order to further study the photodegradation of RhB, the experimental data was fitted according to Eqs. (8) and (9), as shown in Figs. 11 and 12.

The relationships between the photocatalytic equilibrium degradation rate (η_e) and 1/d, and the photocatalytic apparent rate constant (k_{app}) and 1/d are shown in Fig. 12. It displays that at the same diameter, the η_e and k_{app} of spherical nano-CeO_2 are significantly greater than those of linear nano-CeO_2, and the k_{app} has a good linear relationship with the 1/d. This is because adsorption is a necessary step before photocatalysis, the adsorption performance of spherical nano-CeO_2 is better than that of linear nano-CeO_2, and the photocatalytic performance of spherical nano-CeO_2 is also higher than that of linear nano-CeO_2. It can be seen that the photocatalytic performance of nano-CeO_2 is closely related to the adsorption performance.

So such a conclusion can be drawn that the shape and particle size only affects the photocatalytic kinetic parameters of nano-CeO_2, but do not the photocatalytic kinetic order.

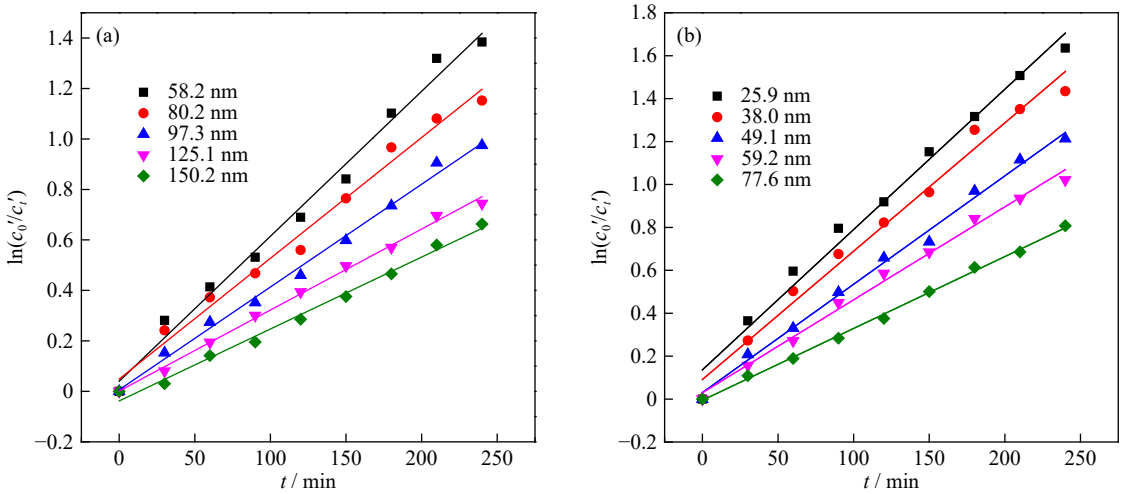

Fig. 10. Fit plots of the Langmuir-Hinshelwood first-order kinetic equation for the photocatalytic degradation of RhB by nano-CeO_2 with different diameters: (a) spherical nano-CeO_2; (b) linear nano-CeO_2.

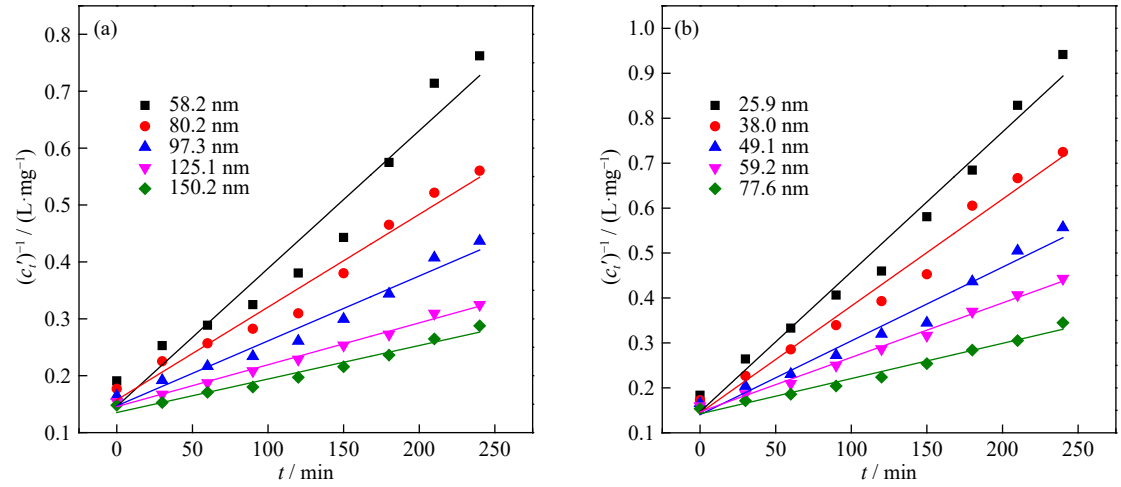

Fig. 11. Fit plots of the second-order kinetic equation for the photocatalytic degradation of RhB by nano-CeO_2 with different diameters: (a) spherical nano-CeO_2; (b) linear nano-CeO_2.

Table 4. Photocatalytic kinetic parameters for photodegradation of RhB by nano-CeO_2

Shape	Size / nm	First-order kinetics		Second-order kinetics	
		k_{app} / min^{-1}	R^2	k_2' / (L·mg^{-1}·min^{-1})	R^2
Spherical nano-CeO_2	58.2	0.00574	0.98712	0.00242	0.94149
	80.2	0.00478	0.98516	0.00163	0.96615
	97.3	0.00407	0.99340	0.00114	0.96390
	125.1	0.00321	0.99603	0.00074	0.99041
	150.2	0.00285	0.99056	0.00059	0.99723
Linear nano-CeO_2	25.9	0.00654	0.98278	0.00311	0.97720
	38.0	0.00598	0.98244	0.00238	0.97554
	49.1	0.00505	0.99369	0.00164	0.96836
	59.2	0.00433	0.99250	0.00121	0.99181
	77.6	0.00335	0.99744	0.00078	0.97798

3.5. Kinetic mechanism of photocatalytic degradation of nanomaterials

3.5.1. Generalized kinetics regularity of adsorption and photocatalytic degradation of nanomaterials

The adsorption processes of RhB by nano-CeO_2 with different shapes and particle sizes agree with the pseudo-second-order adsorption kinetic, while the photocatalytic degradation processes are consistent with the first-order kinetic. The particle size and shape only affect the kinetic parameters of adsorption and photocatalysis. Moreover, a lot of literat-

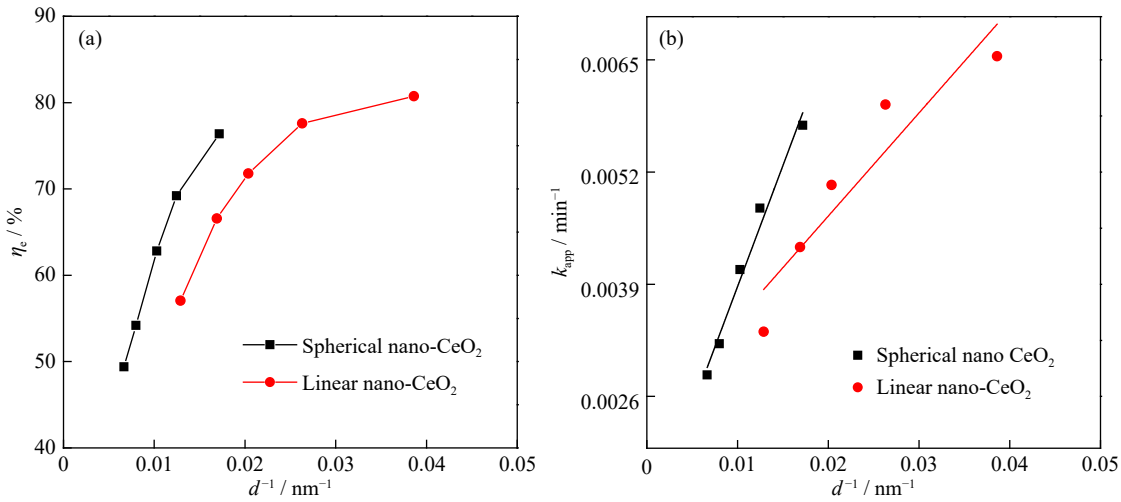

Fig. 12. Relationships between η_e and 1/*d* (a), and k_{app} and 1/*d* (b).

ure has also reported the above kinetic regularities. For example: Wang *et al*. [32] used sol-hydrothermal method to prepare Bi-doped TiO_2 nanocomposites with different molar ratios, and the nanocomposites were used for photocatalytic degradation of antibiotic sulfamethazine; Anirudhan and Deepa [33] introduced nano-ZnO and graphene oxide into the nano-cellulose matrix, and the above material was used for photocatalytic degradation of ciprofloxacin; Raizada *et al*. [34] prepared ZnO activated carbon and ZnO brick particles nanocomposites, and these nanocomposites have good activity of adsorption and photocatalysis for malachite green and Congo red; Priya *et al*. [35] prepared graphene sand composite (GSC) and chitosan (CT) supported BiOCl nanoplates (BiOCl/GSC and BiOCl/CT) by an improved hydrolysis method, and studied the catalytic removal effects of BiOCl/GSC and BiOCl/CT on ampicillin and oxytetracycline; Dutta *et al*. [36] used a simple sonochemical method to synthesize $CuWO_4$ nanoparticles, and these nanoparticles were used for photocatalytic degradation of RhB and malachite green; Popa and Visa [37] prepared a kind of charcoal powder (charcoal prepared from biomass, wastes of the local forest), activated with NaOH solution and with Degussa P25 (TiO_2) was used as adsorbent and photocatalyst for the removal of cadmium cations and methylene blue from wastewater.

Our experimental results are the same as those reported above, which indicates that the adsorption and photocatalytic kinetics of all nanomaterials may have the same kinetic regularity and mechanism. According to the theory of chemical reaction kinetics, all nanomaterials have the same photocatalytic kinetic order, so they should also have the same kinetic mechanism.

3.5.2. Generalized kinetic mechanism of photocatalytic degradation of nanomaterials

According to the above generalized experimental results, a photocatalysis kinetic mechanism of nanomaterials was proposed by us. The photocatalytic kinetic mechanism of nanomaterials can be divided into three elementary steps: the adsorption of a degraded substance in solution on the surface of nanoparticles, the photocatalytic degradation reaction of the adsorbed substance on the surface of nanoparticles, and the desorption of photodegradation products. The rates of the three elementary steps cannot be the same, so there must be the slowest elementary step. The kinetic rate of the whole photocatalytic process depends on the rate of the slowest elementary step. We assume that the rate-controlling step is the adsorption process so that the kinetic order of the overall process of photocatalytic degradation should be the same as the adsorption kinetic order. However, the experimental results are inconsistent with the hypothesis. Therefore, adsorption is not the rate-controlling step. Similarly, since the order of the photochemical reaction kinetics is zero, the photocatalytic reaction is not the rate-controlling step either. So, it can be inferred from the above that the desorption process of the photocatalytic degradation products is the rate-controlling step. The kinetic rate of the overall photocatalytic degradation process is equal to the rate of the desorption process.

The mechanism rate equation of the above-mentioned photocatalytic degradation kinetic mechanism is derived as follows.

It is assumed that the dye molecule B undergoes the following photocatalytic degradation reaction:

$$B \rightleftharpoons d\mathrm{D} + e\mathrm{E} + f\mathrm{F}$$

where D, E, and F are photodegradation products, and *d*, *e*, and *f* are stoichiometric numbers of photodegradation products D, E, and F respectively.

Because the desorption of photodegradation products is the slowest step, relatively speaking, the adsorption rate and the photocatalytic degradation rate are very fast and can reach a rapid equilibrium. The instantaneous concentration is the equilibrium concentration. Therefore, the kinetic mechanism of photocatalytic degradation of nanomaterials can be expressed as follows:

$$\mathrm{B_{sol}} \overset{K_1}{\longleftrightarrow} \mathrm{B_{sur}} \overset{K_2}{\longleftrightarrow} d\mathrm{D_{sur}} + e\mathrm{E_{sur}} + f\mathrm{F_{sur}} \overset{k_3}{\longrightarrow} d\mathrm{D_{sol}} + e\mathrm{E_{sol}} + f\mathrm{F_{sol}}$$

where K_1 and K_2 are equilibrium constants and k_3 is the rate constant. The first two steps are quick balance and the third step is the slowest. The subscripts sol and sur indicate the substances in the solution and adsorbed on the catalyst surface.

$$K_1 = \frac{c_{B(sur)}}{c_{B(sol)}} \quad (10)$$

$$K_2 = \frac{c^d_{D(sur)} c^e_{E(sur)} c^f_{F(sur)}}{c_{B(sur)}} \quad (11)$$

Because the desorption process of the reaction product is an elementary step, it obeys the law of mass action, and the product desorption rate can be expressed as:

$$r_3 = k_3 c^d_{D(sur)} c^e_{E(sur)} c^f_{F(sur)} \quad (12)$$

The rate of the overall photocatalytic degradation process is equal to the rate of product desorption. The mechanism rate equation of the photocatalytic degradation kinetics of nanomaterials can be obtained combined with K_1 and K_2:

$$r = r_3 = k_3 c^d_{D(sur)} c^e_{E(sur)} c^f_{F(sur)} = K_1 K_2 k_3 c_{B(sol)} = k c_{B(sol)} \quad (13)$$

where k is the rate constant of the overall photocatalytic degradation process.

It can be seen from Eq. (13) that the kinetic order of the mechanism rate equation is 1, which is consistent with our experimental results and reported in the literature. Therefore, the photocatalytic degradation kinetic mechanism of the above-mentioned nanomaterials proposed by us is correct and universal, that is to say, all nanomaterials have the same photocatalytic kinetic mechanism and kinetic order.

4. Conclusion

The results show that the shape and particle size have significant effects on the adsorption and photocatalytic kinetics of nanomaterials. With the decreases of particle size, the adsorption rate and logarithm of adsorption rate constant of nano-CeO_2 with the same shape increase gradually, and the photocatalytic degradation rate and photocatalytic degradation rate constant also increase. The adsorption rate, adsorption rate constant, photocatalytic degradation rate, and photocatalytic degradation rate constant of spherical nano-CeO_2 are larger than those of linear nano-CeO_2, and the logarithm of the adsorption rate constant has good linear relationships with the reciprocal of the diameter. However, the particle size and shape do not influence the kinetic order of adsorption and the whole photocatalytic process. On this basis, we proposed a generalized mechanism of photocatalytic kinetics of nanomaterials and derived the mechanism rate equation, which successfully explains the above photocatalysis kinetics and the experimental results in a lot of literature. The kinetic mechanism of photocatalytic degradation is that the photocatalytic kinetic mechanism of nanomaterials can be divided into three elementary steps: the adsorption of a degraded substance in solution on the surface of nanoparticles, the photocatalytic degradation reaction of the adsorbed substance on the surface of nanoparticles, and the desorption of photodegradation products. Among them, the desorption of photodegradation products is the rate-controlling step of photocatalytic kinetics, and the kinetic order of photocatalytic degradation reaction is 1. The photocatalytic degradation kinetic mechanism is universal, that is to say, all nanomaterials have the same photocatalytic kinetic mechanism and kinetic order. The generalized photocatalytic kinetic mechanism of nanomaterials and the effects of shape and particle size on the kinetics of nanomaterial adsorption and photocatalytic degradation proposed by us can provide important guidance and reference for the research and applications of nanomaterials in the field of adsorption and photocatalysis.

Acknowledgements

The work was financially supported by the National Natural Science Foundation of China (Nos. 21373147 and 21573157)

Conflict of Interest

The authors declared that they have no conflicts of interest.

References

[1] S. Tsunekawa, R. Sahara, Y. Kawazoe, and K. Ishikawa, Lattice relaxation of monosize CeO_{2-x} nanocrystalline particles, *Appl. Surf. Sci.*, 152(1999), No. 1-2, p. 53.

[2] L. Zhang, H.C. Teng, J.C. Zhou, Y.M. Sun, N.X. Li, M.C. Liu, and D.W. Jing, Synthesis of AgI/Bi_2MoO_6 nano-heterostructure with enhanced visible-light photocatalytic property, *Prog. Nat. Sci. Mater. Int.*, 28(2018), No. 2, p. 235.

[3] F.P. Yang, Z.Y. Zhang, Y.N. Wang, M.Z. Xu, W. Zhao, J.F. Yan, and C. Chen, Facile synthesis of nano-MoS_2 and its visible light photocatalytic property, *Mater. Res. Bull.*, 87(2017), p. 119.

[4] B.L. Wang, F.C. Yu, H.S. Li, T.Y. Song, D.M. Nan, L. He, H.Y. Duan, S. Wang, and X.X. Tang, The preparation and photocatalytic properties of Na doped ZnO porous film composited with Ag nano-sheets, *Physica E*, 117(2020), art. No. 113712.

[5] S.W. Cao and Y.J. Zhu, Hierarchically nanostructured α-Fe_2O_3 hollow spheres: Preparation, growth mechanism, photocatalytic property, and application in water treatment, *J. Phys. Chem. C*, 112(2008), No. 16, p. 6253.

[6] A. Ahmad, S.H. Mohd-Setapar, C.S. Chuong, A. Khatoon, W.A. Wani, R. Kumar, and M. Rafatullah, Recent advances in new generation dye removal technologies: Novel search for approaches to reprocess wastewater, *RSC Adv.*, 5(2015), No. 39, p. 30801.

[7] Z.Q. Cai, Y.M. Sun, W. Liu, F. Pan, P.Z. Sun, and J. Fu, An overview of nanomaterials applied for removing dyes from wastewater, *Environ. Sci. Pollut. Res.*, 24(2017), No. 19, p. 15882.

[8] B. Kilic, E.B. Simsek, S. Turkdogan, P. Demircivi, Ö. Tuna, S.P. Mucur, and D. Berek, Carbon nanofiber based CuO nanorod counter electrode for enhanced solar cell performance and adsorptive photocatalytic activity, *J. Nanoparticle Res.*, 22(2020), No. 2, p. 1.

[9] S. Vadivel, A.N. Naveen, V.P. Kamalakannan, P. Cao, and N. Balasubramanian, Facile large scale synthesis of Bi_2S_3 nano rods-graphene composite for photocatalytic photoelectrochemical and supercapacitor application, *Appl. Surf. Sci.*, 351(2015), p. 635.

[10] J.S. Appasamy, J.C. Kurnia, and M.K. Assadi, Synthesis and evaluation of nitrogen-doped titanium dioxide/single walled carbon nanotube-based hydrophilic self-cleaning coating layer for solar photovoltaic panel surface, *Sol. Energy*, 196(2020), p.

80.
[11] S.L. Zhou, F. Wang, S. Balachandran, G. Li, X.Q. Zhang, R. Wang, P. Liu, Y.F. Ding, S.M. Zhang, and M.S. Yang, Facile fabrication of hybrid PA6-decorated TiO_2 fabrics with excellent photocatalytic, anti-bacterial, UV light-shielding, and super hydrophobic properties, *RSC Adv.*, 7(2017), No. 83, p. 52375.
[12] R. Zhong, Q. Zhong, M.J. Huo, B.L. Yang, and H. Li, Preparation of biocompatible nano-ZnO/chitosan microspheres with multi-functions of antibacterial, UV-shielding and dye photodegradation, *Int. J. Biol. Macromol.*, 146(2020), p. 939.
[13] Z.F. Xu, J. Chen, and X.T. Zou, Research and analysis of the anti-UV performance of nano-TiO_2 glass beads composite coating, *Integr. Ferroelectr.*, 169(2016), No. 1, p. 73.
[14] X.J. Wen, Q. Lu, X.X. Lv, J. Sun, J. Guo, Z.H. Fei, and C.G. Niu, Photocatalytic degradation of sulfamethazine using a direct Z-Scheme AgI/$Bi_4V_2O_{11}$ photocatalyst: Mineralization activity, degradation pathways and promoted charge separation mechanism, *J. Hazard. Mater.*, 385(2020), art. No. 121508.
[15] J. Sun, C.H. Shen, J. Guo, H. Guo, Y.F. Yin, X.J. Xu, Z.H. Fei, Z.T. Liu, and X.J. Wen, Highly efficient activation of peroxymonosulfate by Co_3O_4/Bi_2WO_6 p-n heterojunction composites for the degradation of ciprofloxacin under visible light irradiation, *J. Colloid Interface Sci.*, 588(2021), p. 19.
[16] J. Guo, C.H. Shen, J. Sun, X.J. Xu, X.Y. Li, Z.H. Fei, Z.T. Liu, and X.J. Wen, Highly efficient activation of peroxymonosulfate by Co_3O_4/Bi_2MoO_6 p-n heterostructure composites for the degradation of norfloxacin under visible light irradiation, *Sep. Purif. Technol.*, 259(2021), art. No. 118109.
[17] C.H. Shen, Y. Chen, X.J. Xu, X.Y. Li, X.J. Wen, Z.T. Liu, R. Xing, H. Guo, and Z.H. Fei, Efficient photocatalytic H_2 evolution and Cr(VI) reduction under visible light using a novel Z-scheme $SnIn_4S_8$/CeO_2 heterojunction photocatalysts, *J. Hazard. Mater.*, 416(2021), art. No. 126217.
[18] C.K. Prier, D.A. Rankic, and D.W.C. MacMillan, Visible light photoredox catalysis with transition metal complexes: Applications in organic synthesis, *Chem. Rev.*, 113(2013), No. 7, p. 5322.
[19] Q. Ling, J.S. Wei, L.Y. Chen, H.J. Zhao, Z. Lei, Z.G. Zhao, R.L. Xie, Q.P. Ke, and P. Cui, Solvothermal synthesis of humic acid-supported CeO_2 nanosheets composite as high performance adsorbent for Congo red removal, *J. Nanosci. Nanotechnol.*, 20(2020), No. 5, p. 3225.
[20] Y.X. Tian, H.Z. Li, Z.Y. Ruan, G.J. Cui, and S.Q. Yan, Synthesis of $NiCo_2O_4$ nanostructures with different morphologies for the removal of methyl orange, *Appl. Surf. Sci.*, 393(2017), p. 434.
[21] R.Q. Gao, Q. Sun, Z. Fang, G.T. Li, M.Z. Jia, and X.M. Hou, Preparation of nano-TiO_2/diatomite-based porous ceramics and their photocatalytic kinetics for formaldehyde degradation, *Int. J. Miner. Metall. Mater.*, 25(2018), No. 1, p. 73.
[22] B. Ji, G.X. Yan, W.F. Zhao, X. Zhao, J.J. Ni, J.L. Duan, Z. Chen, and Z. Yang, Titanium mesh-supported TiO_2 nano-film for the photocatalytic degradation of ethylene under a UV-LED, *Ceram. Int.*, 46(2020), No. 13, p. 20830.
[23] Z. Ghasemi, H. Younesi, and A.A. Zinatizadeh, Kinetics and thermodynamics of photocatalytic degradation of organic pollutants in petroleum refinery wastewater over nano-TiO_2 supported on Fe-ZSM-5, *J. Taiwan Inst. Chem. Eng.*, 65(2016), p. 357.
[24] N. Nasseh, A.H. Panahi, M. Esmati, N. Daglioglu, A. Asadi, H. Rajati, and F. Khodadoost, Enhanced photocatalytic degradation of tetracycline from aqueous solution by a novel magnetically separable $FeNi_3$/SiO_2/ZnO nano-composite under simulated sunlight: Efficiency, stability, and kinetic studies, *J. Mol. Liq.*, 301(2020), art. No. 112434.
[25] S. Lagergren, Zurtheorie der sogenannten adsorption geloster-stoffe, *Kungliga Svenska Vetenskapsakademiens Handlingar*, 24(1898), p. 1.
[26] Y.S. Ho and G. McKay, Pseudo-second order model for sorption processes, *Process. Biochem.*, 34(1999), No. 5, p. 451.
[27] A.T. Nguyen, C.T. Hsieh, and R.S. Juang, Substituent effects on photodegradation of phenols in binary mixtures by hybrid H_2O_2 and TiO_2 suspensions under UV irradiation, *J. Taiwan Inst. Chem. Eng.*, 62(2016), p. 68.
[28] C.H. Nguyen, C.C. Fu, and R.S. Juang, Degradation of methylene blue and methyl orange by palladium-doped TiO_2 photocatalysis for water reuse: Efficiency and degradation pathways, *J. Cleaner Prod.*, 202(2018), p. 413.
[29] M.N. Chong, Z.Y. Tneu, P.E. Poh, B. Jin, and R. Aryal, Synthesis, characterisation and application of TiO_2-zeolite nanocomposites for the advanced treatment of industrial dye wastewater, *J. Taiwan Inst. Chem. Eng.*, 50(2015), p. 288.
[30] Y.Q. Xue, J.P. Du, P.D. Wang, and Z.Z. Wang, Effect of particle size on kinetic parameters of the heterogeneous reactions, *Acta Phys. Chim. Sin.*, 21(2005), No. 7, p. 758.
[31] W.Z. Wang, W. Zhu, and H.L. Xu, Monodisperse, mesoporous $Zn_xCd_{1-x}S$ nanoparticles as stable visible-light-driven photocatalysts, *J. Phys. Chem. C*, 112(2008), No. 43, p. 16754.
[32] N. Wang, X. Li, Y.L. Yang, T.T. Guo, X.X. Zhuang, S.Y. Ji, T.T. Zhang, Y. Shang, and Z.W. Zhou, Enhanced photocatalytic degradation of sulfamethazine by Bi-doped TiO_2 nano-composites supported by powdered activated carbon under visible light irradiation, *Sep. Purif. Technol.*, 211(2019), p. 673.
[33] T.S. Anirudhan and J.R. Deepa, Nano-zinc oxide incorporated graphene oxide/nanocellulose composite for the adsorption and photo catalytic degradation of ciprofloxacin hydrochloride from aqueous solutions, *J. Colloid Interface Sci.*, 490(2017), p. 343.
[34] P. Raizada, P. Singh, A. Kumar, G. Sharma, B. Pare, S.B. Jonnalagadda, and P. Thakur, Solar photocatalytic activity of nano-ZnO supported on activated carbon or brick grain particles: Role of adsorption in dye degradation, *Appl. Catal. A*, 486(2014), p. 159.
[35] B. Priya, P. Shandilya, P. Raizada, P. Thakur, N. Singh, and P. Singh, Photocatalytic mineralization and degradation kinetics of ampicillin and oxytetracycline antibiotics using graphene sand composite and chitosan supported BiOCl, *J. Mol. Catal. A Chem.*, 423(2016), p. 400.
[36] D.P. Dutta, A. Rathore, A. Ballal, and A.K. Tyagi, Selective sorption and subsequent photocatalytic degradation of cationic dyes by sonochemically synthesized nano $CuWO_4$and $Cu_3Mo_2O_9$, *RSC Adv.*, 5(2015), No. 115, p. 94866.
[37] N. Popa and M. Visa, The synthesis, activation and characterization of charcoal powder for the removal of methylene blue and cadmium from wastewater, *Adv. Powder Technol.*, 28(2017), No. 8, p. 1866.